Scilight

Energy Safety Science and Technology
https://www.sciltp.com/journals/esst

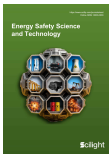

Article

Research on the Evolution Characteristics of Soil-Covered Liquefied Petroleum Gas Leakage and Explosions

Jiang Pu [1,2,†], Yawei Lu [3,†], Dan Li [4], Yi Xie [1,2], Zhiqiang Ge [1,2] and Zhirong Wang [3,*]

[1] Special Equipment Safety Supervision Inspection Institute of Jiangsu Province, Nanjing 210036, China
[2] Key Laboratory of Risk Control Technology of Process Equipment for Jiangsu Province Market Regulation, Nanjing 210036, China
[3] School of National Safety and Emergency Management, Nanjing Tech University, Nanjing 211816, China
[4] College of Chemical Engineering, Nanjing Tech University, Nanjing 211816, China
* Correspondence: wangzhirong@njtech.edu.cn
† These authors contributed equally to this work.

How To Cite: Pu, J.; Lu, Y.; Li, D.; et al. Research on the Evolution Characteristics of Soil-Covered Liquefied Petroleum Gas Leakage and Explosions. *Energy Safety Science and Technology* **2026**, *1*(1), 2.

Received: 14 April 2026
Revised: 26 April 2026
Accepted: 29 April 2026
Published: 7 May 2026

Abstract: To investigate the effect of soil cover thickness on the combustion and explosion behavior of buried liquefied petroleum gas leakage, an experimental system for underground leakage-induced combustion and explosion was established. Four soil cover thicknesses of 80 mm, 120 mm, 160 mm and 200 mm were set to record flame propagation and temperature field evolution. The results show that the flame undergoes four stages: initial ignition, rapid expansion, full combustion and decay extinction. Under 80 mm soil cover, the flame exhibits upper-lower separation, with the lowest peak height (873.9 mm). At 160 mm, the peak flame height reaches the maximum (1408.1 mm) and occurs earliest. At 200 mm, the premixing is most sufficient, giving the highest peak temperature (1406.5 °C), but the peak appears latest and decays most slowly. Soil cover thickness significantly influences flame morphology, height, temperature and decay characteristics. These findings provide a theoretical basis for the safety design and risk prevention of buried liquefied petroleum gas systems.

Keywords: liquefied petroleum gas; buried leakage; soil cover thickness; flame propagation; temperature field

1. Introduction

With the accelerated transformation of energy consumption toward cleaner and lower-carbon sources, the share of natural gas and liquefied hydrocarbon energy products in total consumption has continued to rise, and both the scale of pipeline construction and the number of storage tanks in operation have expanded rapidly. Against a backdrop of increasingly dense pipeline networks and storage tank facilities, buried pipelines and soil covered storage tanks are widely used due to their unique engineering advantages, but they also face common and serious safety challenges.

Scholars have systematically studied the evolution of the leakage and diffusion of combustible media in soil covered storage tanks and pipelines through experiments and numerical simulations. Yan et al. [1] conducted experimental research on buried pipeline leaks under different hydrogen blending ratios, leakage pressures and leakage directions. The applicability of the gas leakage mass flow model was verified. The effect of blending ratio and leakage direction on the methane diffusion range was revealed. Furthermore, a quantitative relationship between leakage concentration and diffusion distance was established. Deborah et al. [2] investigated the critical conditions governing the formation of pothole and gas diffusion during hydrogen and methane leakage. It was found that pothole was more likely to form when the leakage pressure was higher and the gas flows upward, whereas when the pressure was lower or the gas flows downward, the gas primarily diffused through the soil. Zhu

et al. [3] revealed through experimental studies the positive correlation between the diffusion range and the proportion of a single component as well as the pipeline pressure, and established a functional relationship between the leakage concentration and the diffusion distance. Yan et al. [4] conducted experimental research on methane leakage under different flow rates and leakage directions, revealing an inverse relationship between flow rate and both the concentration saturation time and steady-state concentration in methane leakage from buried pipelines. It was identified that concentrations increase most rapidly near the surface, while steady state concentrations were highest below the pipeline. Latifi et al. [5] conducted experiments to reveal the relationship between soil particle size, dry bulk density, permeability coefficient and the leakage flow rate through pipeline cracks, and determined that D50, dry bulk density and permeability coefficient were the most suitable parameters for characterizing the influence of soil on leakage. Hibi et al. [6] conducted experimental studies on methods for determining gas diffusion and dispersion parameters in soils with varying permeability, revealing a quadratic relationship between the dispersion coefficient and the molar fraction of the tracer gas. Zhang et al. [7] used numerical simulations to investigate the effects of factors such as leak hole diameter, soil type and pipeline pressure on the diffusion behavior of buried hydrogen leaks. It was found that hydrogen concentration exhibited symmetric distribution over time, the increase in pipeline pressure caused longitudinal diffusion to gradually become dominant and both the diffusion rate and range of hydrogen in sandy soil were greater than those in clay. Peng et al. [8] demonstrated that porosity was a key factor determining the diffusion rate of hydrogen-blended natural gas. It was established that hydrogen diffused most rapidly in clay and most slowly in loam, and that the time required for diffusion to the surface was highly sensitive to burial depth. Liu et al. [9] revealed the synergistic mechanisms of leak location, wind speed, and obstacles on hydrogen diffusion pathways and the distribution of hazardous zones. Yuan et al. [10] identified the leakage hole diameter as the dominant factor influencing the distance of hydrogen diffusion, as well as the regulatory effects of wind speed and temporal evolution on diffusion in low-concentration zones. Wagih et al. [11] revealed the mechanisms governing the effects of hydrogen blending ratios, pipeline pressure, leakage hole size and soil porosity on diffusion behavior and surface detection time. Wang et al. [12] further established an exponential relationship between the critical time for methane leakage from buried pipelines and the dispersion distance, along with a predictive equation.

Wang et al. [13,14] discovered through numerical simulation that risk areas were positively correlated with the leakage hole size and pipeline pressure. Soil particle size and porosity directly determined the concentration distribution, and the diffusion range in sandy soil was larger than that in clay soil. Ebrahimi et al. [15] simulated the leakage and diffusion of natural gas in soil. The results indicated that gas within buried pipelines flows at the speed of sound near the leakage point, whereas it flowed at subsonic velocity in the soil. Subsequently, a three-dimensional model was developed to simulate leakage in buried gas pipelines, demonstrating that the three-dimensional model provides a more accurate representation of leakage than the two-dimensional model of buried pipelines [16]. Liu et al. [17] developed models for estimating leakage rates and predicting methane concentrations in buried natural gas pipelines using a combination of experimental and numerical simulation methods. It was also revealed the nonlinear relationship between leakage rates and pressure, hole size, soil porosity and particle size.

Scholars have also conducted systematic research on the consequences of leakage accidents involving buried storage tanks and pipelines. Wang et al. [18] revealed the regulatory mechanisms of wind speed in urban environments on the dispersion range of natural gas pipeline leaks, explosion overpressure, and the distribution of jet fire radiation through numerical simulations. Zhao et al. [19] developed a model for calculating leakage rates by analyzing the dynamic leakage process in gas pipelines. It was revealed that factors such as leakage hole diameter and wind speed influence the maximum diffusion concentration and the area susceptible to poisoning and explosion. Hu et al. [20] revealed the failure mechanism of leakage caused by stress concentration in ultra-deep buried gas pipelines under the combined effects of soil corrosion and environmental loads through field testing and numerical simulation. Zhang et al. [21] demonstrated through simulation that the downwind location of a tank leakage played a decisive role in determining the severity of the consequences. It was further noted that pulsating flow can affect the height of the toxic zone and the toxic dose to pedestrians by as much as 30–40%. In terms of engineering practice and risk analysis, Ikwan et al. [22] combined fault tree analysis, risk matrices and dynamic modeling to demonstrate that dynamic risk models can quantify the probability of storage tank leaks in real time and improve decision-making accuracy through multi-factor coupling analysis. Yu et al. [23] revealed the failure modes with the highest risk of rupture and the lowest risk of design defects in liquefied natural gas storage tanks by refining the FMEA model. Wu et al. [24] used digital twin modeling and machine learning methods to demonstrate that the developed model can accurately map the state of liquefied natural gas storage tanks and effectively predict the evolution of leakage zones. Currently, scholars have conducted extensive research on leakages from buried pipelines and storage tanks. However, these researches primarily focused on the dispersion patterns, key influencing factors and risk assessment methods for natural gas, hydrogen and hydrogen-

blended gas leaks. There has been relatively little research on liquefied petroleum gas. Current research mostly focused on the overall structure of buried pipelines or storage tanks, with relatively little attention paid to localized failure modes such as buried leaks. There was a notable lack of systematic research on combustion and explosion behavior after leakage. Furthermore, soil depth was a key structural parameter for underground leakage, the mechanism by which it influenced the combustion and explosion behavior of liquefied petroleum gas after leakage was still unclear. There was also a lack of systematic experimental support for the quantitative relationship between changes in leakage flow rate and the risk of combustion and explosion.

Therefore, this work investigates the combustion and explosion behavior of liquefied petroleum gas leakage by varying the soil depth, revealing the influence of soil depth on the propagation of explosion flames and the evolution of flame temperature fields. The research findings can provide theoretical foundations and technical support for the safe design, risk management, and emergency response of buried liquefied petroleum gas systems.

2. Experimental Setup

The experimental procedure utilized an underground gas leakage and explosion test system. The system comprises a square vessel, a gas distribution system, an ignition system, a synchronization control system and a data acquisition system, the experimental setup is shown in Figure 1. The size of the square vessel is 540 mm × 380 mm and is filled with soil. To minimize the influence of soil properties on the experimental results, soil samples were taken from the tank farm area and used in the experiments, thereby ensuring consistent soil conditions. The large impurities in the soil sample were sieved out using a sieve, and the sample was then spread evenly above the leakage port. The soil selected for the experiment was sandy soil, with an initial moisture content of 6.5%, a porosity of 0.310 and a density of 2.40 g/cm^3. During the experiment, the soil cover thicknesses were set at 80 mm, 120 mm, 160 mm and 200 mm. The leakage port is a circular opening with a diameter of 10 mm; it is located at the center of the bottom of the vessel and is flush with the inner surface of the vessel. The flow rate of liquefied petroleum gas was precisely controlled using a mass flow meter. In the experiments, the flow rate was set to 30 L/min. The ignition of the leakage gas was achieved using a high-precision automatic ignition controller; the ignition electrode was positioned at the center of the soil surface, and the ignition energy was 2 J. Gas supply was cut off 30 s after the leak began and ignition was initiated simultaneously; the ignition duration was 100 ms, which remained consistent throughout all experiments. The high speed camera is used to capture the propagation patterns of the explosion flame, with a frame rate of 50 Hz. The high speed infrared thermal camera is used to record the evolution of the explosion flame temperature field, with a frame rate of 100 Hz. During data acquisition, the emissivity was set to 0.7. To extract flame morphological parameters, the video from the high-speed camera is exported frame by frame as color images, then converted to grayscale images, and finally subjected to binarization. By comparing the original image with the binary image, the threshold is selected such that the white regions most closely match the actual flame contours. To ensure the reproducibility of the experiment and the accuracy of the results, each set of experiments was repeated three times. It was found through comparison that maximum errors of the maximum flame height and the maximum flame temperature were 4.8% and 6.2%.

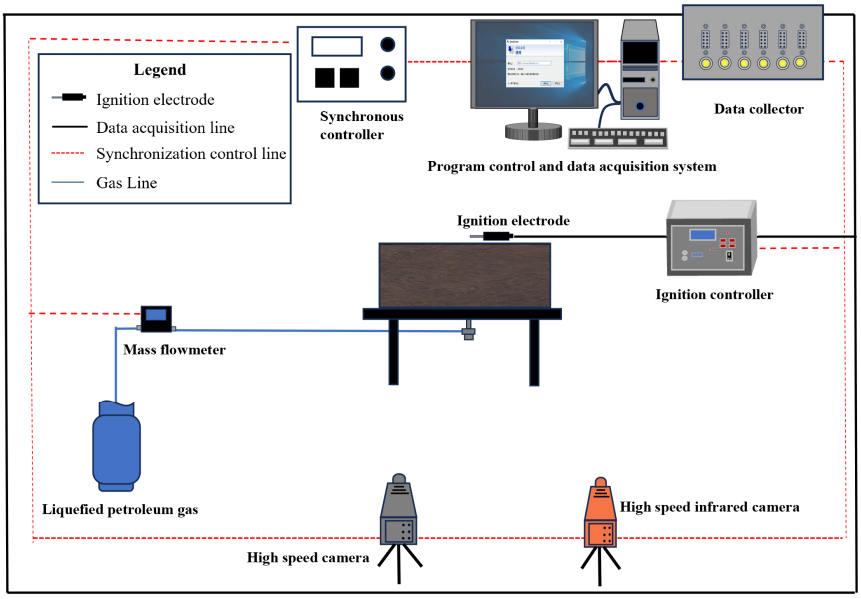

Figure 1. Schematic diagram of the experimental apparatus.

3. Results and Discussion

3.1. Flame Propagation Patterns

Figure 2 shows the propagation and evolution of a flame resulting from a liquefied petroleum gas leak and explosion under conditions of 80 mm soil cover. It can be observed that the flame undergoes four stages from ignition to extinction: the initial ignition stage, the rapid expansion stage, the full combustion stage, and the decay and extinction stage. At 60 ms after ignition, the flame height was only 39.4 mm; the flame was confined to the vicinity of the ignition source, appearing as an isolated small flame cluster with an irregular pattern. At 160 ms, the flame height reached 97.5 mm, and the flame spread rapidly in all directions, forming a flat structure [25]. At 240 ms, the flame reached a height of 217.5 mm, taking on a flat, mushroom-like shape with its base completely covering the soil layer. At 320 ms, the flame height increased to 354.4 mm; the center of the flame bulged outward, and the flame began to shift from spreading laterally to rising vertically. The flame height increased further to 487.5 mm at 400 ms, with a distinct bulge appearing at the top of the flame and a broad base at the bottom. The flame reached its maximum height of 873.8 mm at 740 ms, forming a columnar structure with irregular branching at the top, exhibiting the characteristics of fully developed turbulent combustion. The flame height dropped slightly to 845.6 mm at 780 ms, but the flame fractured into upper and lower segments, with the originally continuous columnar flame splitting into two separate fire clusters. The propagation of flames was influenced by buoyancy, resulting in flame pulsations and vortices [26–28]. Meanwhile, differences in density and velocity between the flame and the surrounding air caused instability in the flame flow. Opposing vortices were formed at the inner and outer of the flame due to the effects of shear-layer perturbation and gravity [29]. The stretch and compression on the flame surface by the inner and outer vortices lead to radial pulsation. The 80 mm soil cover exerted minimal resistance to gas flow; in the early stage of leakage, gas rapidly seeped out, creating a high-concentration supply. After the peak, the supply rate dropped sharply. The bottom flame weakened due to fuel depletion, while the upper flame continued to rise under buoyancy. In the middle of the flame column, the flame neck contracted and ruptured due to Rayleigh-Taylor instability and the interpenetration of fluid regions with different densities [30]. After the rupture, the upper part of the flame detached from the fuel source and quickly extinguished, while the bottom part continued to burn due to residual gas. Compared to soil cover depths of 120 mm, 160 mm, and 200 mm, the 80 mm depth had the minimum peak height and the fastest decay rate, and was the only condition in which the flame broke up at both the top and bottom [31].

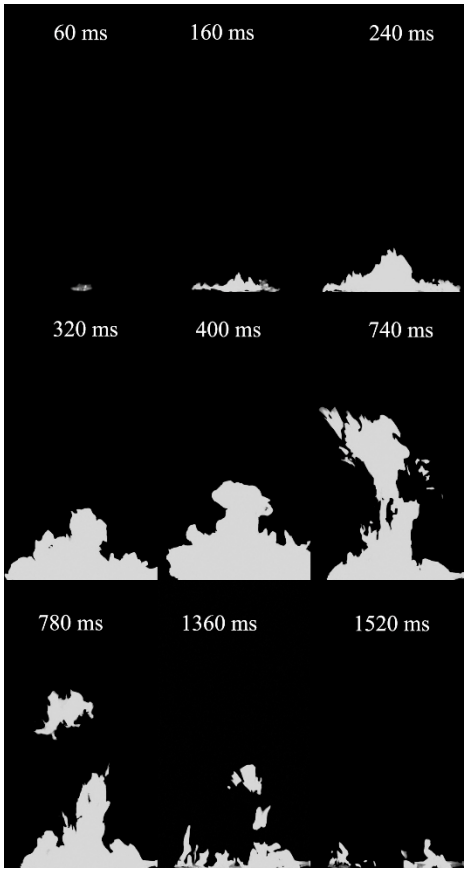

Figure 2. Flame patterns during combustion and explosion with the 80 mm soil cover.

Figure 3 shows the propagation process of a flame resulting from a liquefied petroleum gas leak and explosion under conditions of 120 mm soil cover. At 80 ms after ignition, the flame height was 11.3 mm. The flame height reached 78.8 mm at 160 ms, and the flame began to spread outward. At 240 ms, the flame height reached 245.6 mm, and the flame flattened out and covered the soil layer. The flame height increased to 273.8 mm at 320 ms, the flame bulged in the middle and began to propagate vertically. At 600 ms, the flame height rapidly increased to 1046.3 mm, and the flame formed a distinct columnar structure with branching at the top. The flame height reached a maximum of 1059.4 mm at 740 ms; the columnar structure was even more pronounced than at 800 ms, and the branching at the top and the serrated edges were more evident. The flame height decreased to 905.6 mm at 820 ms; the flame began to diminish, but the columnar structure still persisted. The flame height further decreased to 408.7 mm at 1520 ms, and the flame gradually became thinner. The flame height decreased to 395.6 mm at 1680 ms, a reduction of 62.7% compared to the maximum flame height. The flame height decreased by 663.8 mm from 740 ms to 1680 ms, while the 80 mm soil cover decreased by 730.0 mm from 740 ms to 1520 ms. Under the 120 mm soil cover, the gas release rate remained relatively stable before and after the peak, with no abrupt drop-off, allowing the flame column to remain continuous for a longer period [32]. Furthermore, under the 120 mm conditions, no vertical fragmentation of the flame occurred; the flame column remained continuous throughout the decay stage and only gradually fragmented after 1700 ms. The flame gradually extinguished in the later stage; it became unstable due to buoyancy, which led to the phenomenon of flame cracking.

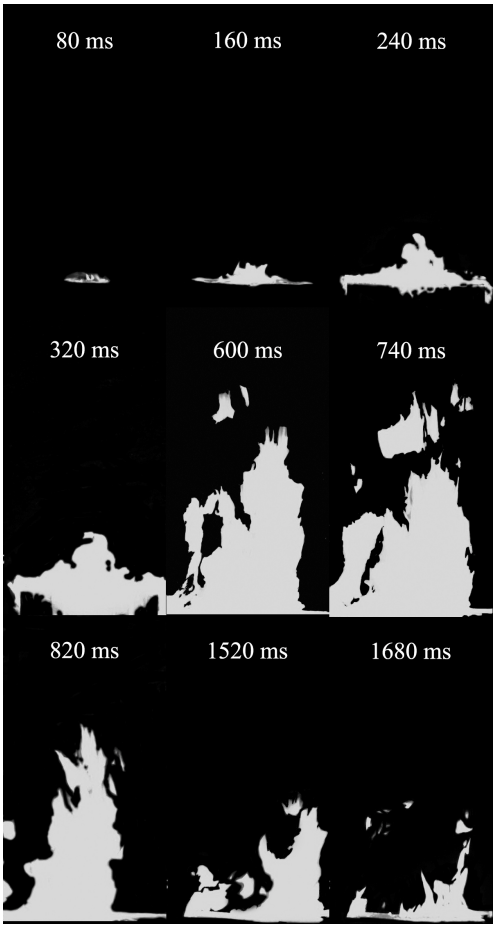

Figure 3. Flame patterns during combustion and explosion with the 120 mm soil cover.

Figure 4 shows the propagation process of a flame resulting from a liquefied petroleum gas leak and explosion under conditions of 160 mm soil cover. At 60 ms after ignition, the flame height reached 97.5 mm, which was higher than the values recorded at the same time for soil cover of 80 mm and 120 mm. Although a greater soil cover depth delayed the arrival of liquid petroleum gas at the surface, the gas remained in the soil pores for a longer period, allowing for more thorough premixing with air. As a result, the seeping flammable mixture exhibited greater uniformity and reactivity [33]. The flame height reached 243.8 mm, 262.5 mm, 658.1 mm, and 860.6 mm at 220 ms, 260 ms, 460 ms and 500 ms, respectively, and reached the maximum of 1408.1 mm at 700 ms. The flame formed a pronounced columnar structure with distinct branching at the top, exhibiting the characteristics of fully developed turbulent combustion. The maximum flame height was 1408.4 mm when the soil cover was 160 mm

thick, but it occurred earlier, at 700 ms. Meanwhile, due to the relatively steady release rate, the flame did not break up during the decay process. The flame height decreased to 491.2 mm and 258.8 mm at 1540 ms and 1900 ms respectively, representing reductions of 65.1% and 81.6% compared with the maximum flame height. Compared with the 120 mm soil cover, the peak height of 160 mm was approximately 348.8 mm higher.

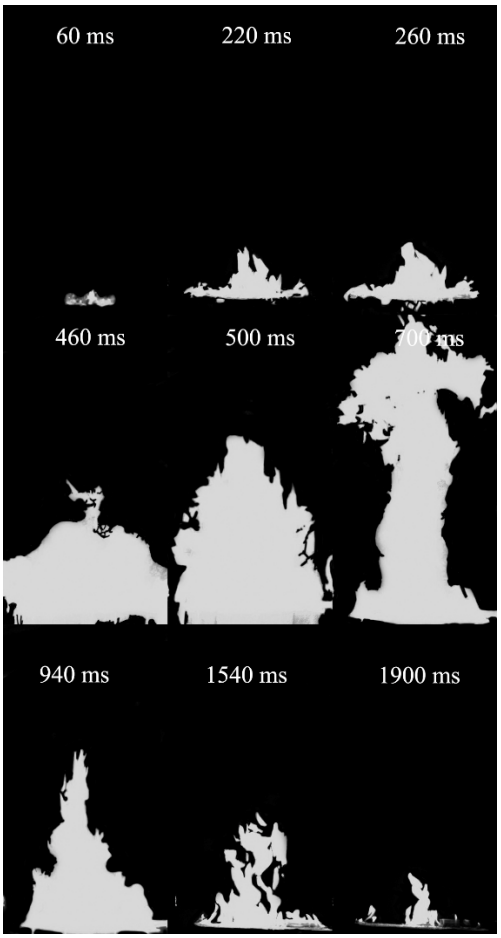

Figure 4. Flame patterns during combustion and explosion with the 160 mm soil cover.

Figure 5 shows the propagation process of a flame resulting from a liquefied petroleum gas leak and explosion under conditions of 200 mm soil cover. At 80 ms after ignition, the flame height was 116.3 mm, with an initially relatively high height. This indicated that under 200 mm of soil cover, the degree of premixing of the gas within the soil had reached an optimum, and the permeating combustible mixture possessed the highest reactivity. The flame height reached 275.6 mm, 367.5 mm, 740.6 mm, and 898.1 mm at 160 ms, 220 ms, 400 ms and 560 ms, respectively, and reached the maximum of 1398.8 mm at 840 ms [34]. Soil was a complex porous medium, and the structure of the porous medium became increasingly complex as the soil cover thickness increased. With the soil cover thickness increased to 160 mm and 200 mm, there was little difference in the maximum flame height. The soil cover thickness increased the degree of gas premixing, but it also increased the resistance to gas diffusion. Increasing the soil cover thickness had a significant effect on the duration of the flame, but had little effect on the maximum flame height to a certain extent. The flame heights decreased to 1230.0 mm, 763.1 mm and 240.1 mm at 940 ms, 1620 ms and 2220 ms respectively. When the soil cover was 200 mm, the peak height occurred later, at 840 ms. The thicker soil cover resulted in a significant increase in pressure at the leak point and greater soil resistance, meaning it took longer for the gas to seep out in significant quantities. Meanwhile, the rate of decline after the peak was the slowest of the four groups; the flame height decreased by 1158.8 mm from 840 ms to 2220 ms, whereas it decreased by 1149.5 mm from 700 ms to 1900 ms when the soil cover was 160 mm. This gradual decay was due to the low but steady gas release rate under the thick soil cover, which allowed the flame to maintain a high combustion intensity even after reaching its peak.

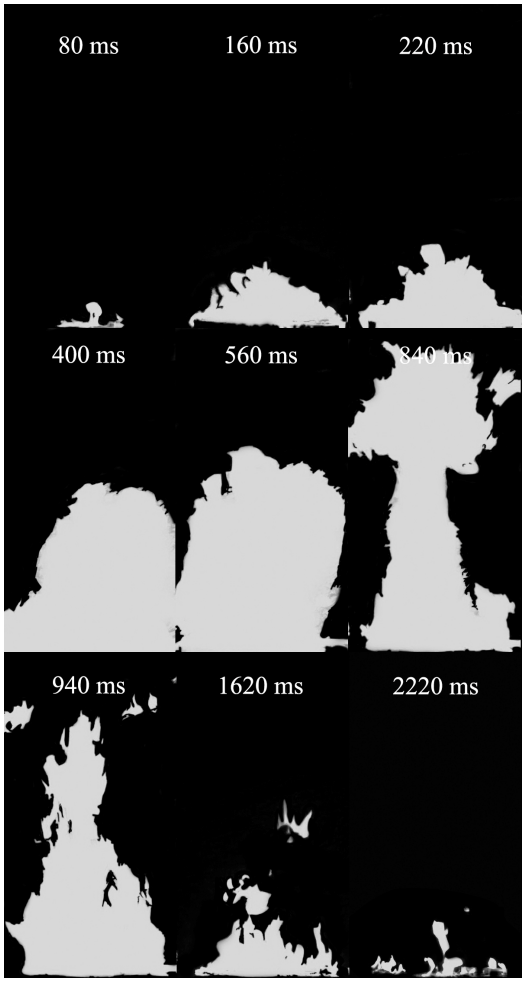

Figure 5. Flame patterns during combustion and explosion with the 200 mm soil cover.

3.2. Flame Temperature Distribution

Figure 6 shows the evolution of the flame temperature field during a liquefied petroleum gas leak and explosion under conditions of 80 mm of soil cover. At 60 ms after ignition, the maximum temperature was 863.6 °C. At 120 ms, the flame spread outward, the heat release rate increased, and the maximum temperature increased to 895.4 °C. The flame had developed into a flat mushroom shape by 220 ms, completely covering the soil layer; internal turbulent mixing intensified, and the maximum temperature further increased to 1021.9 °C. The temperature reached a maximum of 1284.0 °C at 360 ms. The flame began to shift from spreading laterally to rising vertically. Liquefied petroleum gas was released in large quantities from the soil, and fresh air was drawn in simultaneously from the sides and bottom of the flame, creating an optimal mixture of fuel and air [35]. Meanwhile, the turbulence within the flame was moderate, ensuring a steady supply of fuel while preventing heat loss caused by excessive entrainment. At 420 ms, the flame began to stretch upward; as the concentration decreased, convective and radiative heat loss increased due to the increasing flame surface, causing the maximum temperature decrease to 1197.0 °C. The maximum temperature decreased to 927.5 °C at 800 ms, and the flame took on a slender shape. At 860 ms, the discontinuity in the supply of liquefied petroleum gas under conditions of a thin soil cover caused the flame to fracture into upper and lower segments, and the maximum temperature decreased to 892.3 °C. This was because the 80 mm soil provided very little resistance to gas flow; gas rapidly seeped out during the initial stages of a leak, creating a high-concentration supply, but the supply rate decreased sharply once the peak was reached. The lower part of the flame weakened due to a decrease in concentration, while the upper part continued to propagate upward under the influence of buoyancy, causing the middle part of the flame column to constrict and fracture due to Rayleigh-Taylor instability. The upper portion of the flame extinguished rapidly after the rupture due to a lack of fuel, while the lower portion continued to combust at a low temperature, sustained by residual gas. The maximum flame temperature then gradually decreased, reaching 848.5 °C and 649.0 °C at 1320 ms and 1500 ms, respectively, representing decreases of 34.0% and 49.5% from the peak flame temperature.

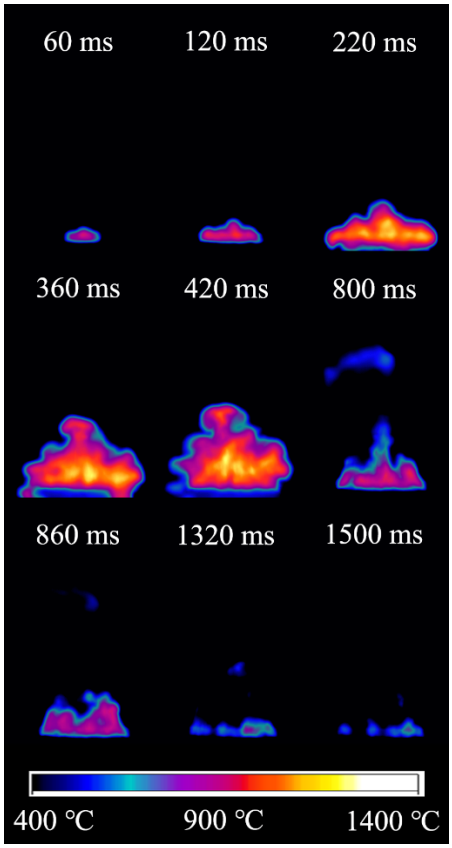

Figure 6. Flame temperature distribution under the 80 mm soil cover.

Figure 7 shows the evolution of the flame temperature field during a liquefied petroleum gas leak and explosion under conditions of 120 mm of soil cover. The maximum flame temperatures were 878.3 °C, 963.2 °C, and 1155.0 °C at 80 ms, 120 ms, and 280 ms, respectively. The highest flame temperature reached a maximum of 1306.5 °C at 400 ms. As with the 80 mm soil cover, the peak flame temperature occurred at the transition point from lateral spread to vertical rise, but the maximum temperature was approximately 22.5 °C higher than that observed with the 80 mm soil cover. This was because the gas took longer to pass through the soil, allowing it to accumulate more evenly in the soil pores, which resulted in a higher heat release rate. The flame height increased rapidly at 660 ms, but the temperature decreased to 1286.3 °C. This indicated that even if the flame was rapidly elongated, the gas supply remained steady and continued to provide the flame with sufficient fuel. At 880 ms, the maximum flame temperature decreased to 1030.5 °C. Compared to the same time at 80 mm, the temperature at 120 mm was approximately 103.0 °C higher, indicating that the gas supply under the intermediate soil cover was able to maintain a high combustion efficiency even after the flame had elongated. The maximum flame temperature decreased to 993.8 °C, 961.2 °C, and 770.4 °C at 1080 ms, 1420 ms, and 1700 ms, respectively. When the soil cover was 120 mm, the temperature decline rate after the maximum temperature occurred was significantly slower than when the soil cover was 80 mm. The maximum flame temperature decreased by 276.0 °C from 400 ms to 660 ms, whereas it decreased by 357.0 °C during the same period when the soil cover was 80 mm [36]. When the soil cover was 120 mm, the gas release rate remained relatively stable before and after the peak, resulting in a relatively gradual heat release rate [37].

Figure 8 shows the evolution of the flame temperature field during a liquefied petroleum gas leak and explosion under conditions of 160 mm of soil cover. The maximum flame temperatures were 886.4 °C, 1083.9 °C, and 1197.1 °C at 60 ms, 140 ms, and 300 ms, respectively. At 460 ms, the maximum temperature reached its peak of 1336.5 °C. Unlike the 80 mm and 120 mm soil cover thicknesses, the maximum flame temperature for the 160 mm soil cover occurred later, at 460 ms. Furthermore, the maximum flame temperature was higher than the soil cover of 80 mm and 120 mm. This was because the increased of the soil cover significantly increased the resistance to the liquefied petroleum gas passing through the soil, thereby delaying the moment when the liquefied petroleum gas seeped out in large quantities and formed an optimal mixture, and also increasing the heat release rate [38,39]. The maximum flame temperatures were 1293.9 °C, 1112.4 °C, 1040.1 °C, and 1054.9 °C at 540 ms, 730 ms, 960 ms, and 1600 ms, respectively. The maximum flame temperature rose slightly at 1600 ms, possibly due to the

secondary combustion of unburned gas following flame fragmentation; however, the overall decay trend remained unchanged. At 1980 ms, the maximum flame temperature decreased to 684.4 °C.

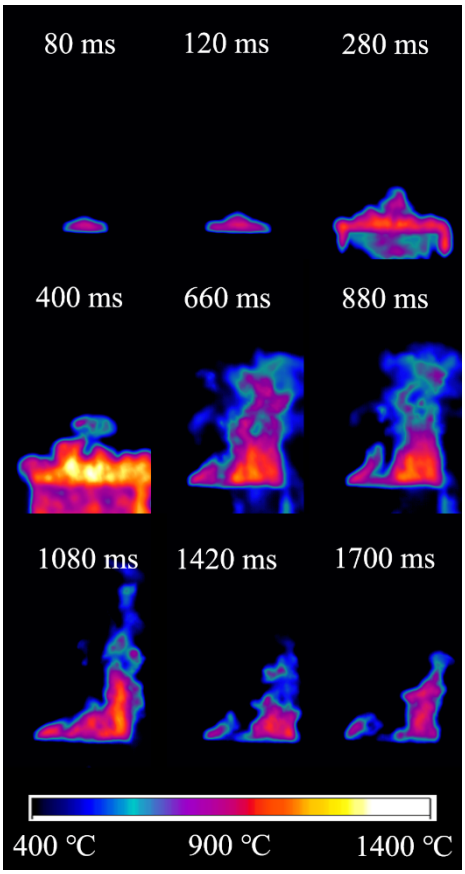

Figure 7. Flame temperature distribution under the 120 mm soil cover.

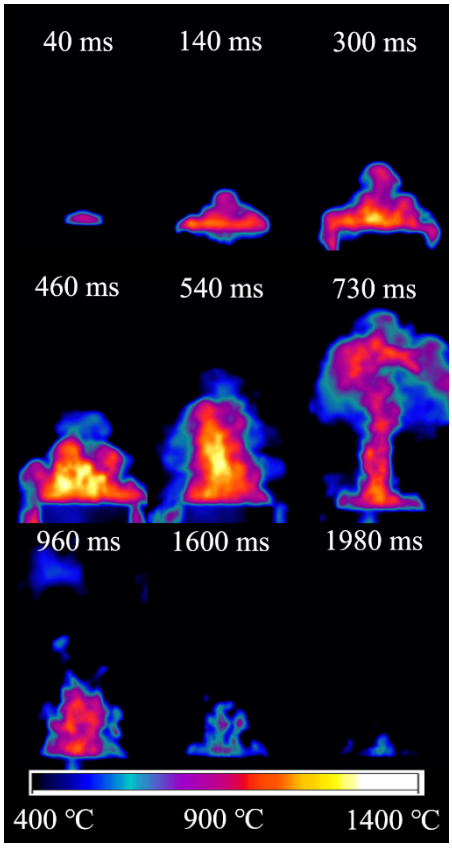

Figure 8. Flame temperature distribution under the 160 mm soil cover.

Figure 9 shows the evolution of the flame temperature field during liquefied petroleum gas leak and explosion under condition of 200 mm of soil cover. At 60 ms after ignition, the maximum flame temperature was 908.6 °C, which was higher than that observed for other soil cover. This indicated that under a 200 mm soil cover, the degree of premixing of the liquefied petroleum gas in the soil was optimal, and the permeating mixture exhibited the highest reactivity. Maximum flame temperature reached maximum value of 1406.5 °C at 400 ms, this occurred 60 ms earlier than the soil cover was 160 mm. When the soil cover was 200 mm, the maximum flame temperature was 122.5 °C, 100.0 °C, and 70.0 °C higher than when the soil cover were 80 mm, 160 mm, and 200 mm, respectively. This was because the gas had the longest propagation path and the most thorough premixing time when the soil cover was 200 mm, resulting in optimal uniformity and concentration of the combustible mixture [40]. In addition, a greater thickness of soil cover resulted in a significant increase of pressure on the leak point, causing the gas to leak at a faster rate. The maximum flame temperatures decreased to 1388.86 °C, 1245.6 °C, 1198.2 °C, 1099.4 °C, and 659.7 °C at 600 ms, 890 ms, 1100 ms, 1520 ms, and 2170 ms, representing decreases of 1.3%, 11.4%, 14.8%, 21.8% and 53.1% compared to the peak flame temperature.

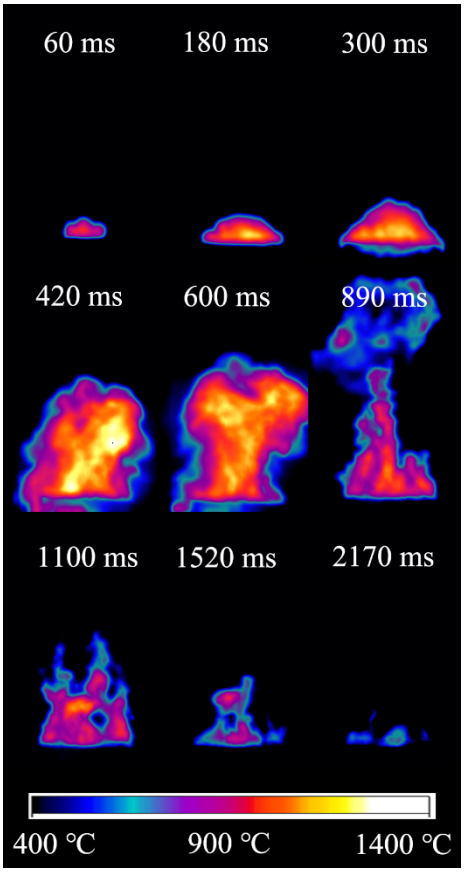

Figure 9. Flame temperature distribution under the 200 mm soil cover.

4. Conclusions

This study experimentally investigated the propagation patterns of combustion and explosion flames and the evolution of temperature fields following underground liquefied petroleum gas leaks by varying the thickness of the soil cover (80 mm, 120 mm, 160 mm, and 200 mm). The main conclusions are as follows:

(1) Regardless of the thickness of the soil cover, flames always go through an initial ignition stage, a rapid expansion stage, a full combustion stage, and a decay and extinction stage. When the soil cover was 80 mm, a neck-down fracture occurred in the middle of the flame column due to Rayleigh-Taylor instability, resulting in the separation of the upper and lower sections. When the soil cover was 120 mm or thicker, the gas release rate remained relatively stable, and the flame column remained continuous without any interruptions. With the soil cover increased from 80 mm to 160 mm, the maximum flame height gradually increased. However, the maximum flame height at a soil cover of 200 mm was only marginally different from 160 mm.

(2) With the increase in the soil cover depth, the maximum flame temperature gradually increased. The maximum flame temperature increased from 1284.0 °C to 1406.5 °C with the soil cover depth increasing from 80 mm to 200 mm. Through comparative analysis of the late-stage flame temperature decay process, it can be

observed that as the soil cover depth increased, the temperature decay gradually slowed down and the combustion duration became longer.

Author Contributions

J.P.: Data curation, writing—original draft preparation; Y.L.: Conceptualization, methodology, data curation, writing—original draft preparation; D.L.: Software, data curation, writing—original draft preparation; Y.X.: Validation, writing—reviewing and editing; Z.G.: Validation, writing—reviewing and editing; Z.W.: Visualization, investigation, supervision, validation, writing—reviewing and editing. All authors have read and agreed to the published version of the manuscript.

Funding

This work was funded by the National Key R&D Program of China (2024YFC3013701), National Natural Science Foundation of China (52404219, 52274210) and Research on Basic Science (Natural Science) in Higher Education Institutions of Jiangsu Province No. 24KJB620005.

Institutional Review Board Statement

Not applicable.

Informed Consent Statement

Not applicable.

Data Availability Statement

The data that support the findings of this study are available from the corresponding author upon reasonable request.

Conflicts of Interest

The authors declare no conflict of interest. Given the role as Editor-in-Chief, Z.W. had no involvement in the peer review of this paper and had no access to information regarding its peer-review process. Full responsibility for the editorial process of this paper was delegated to another editor of the journal.

Use of AI and AI-Assisted Technologies

No AI tools were utilized for this paper.

References

1. Yan, Y.T.; Zhang, H.R.; Li, J.M.; et al. Simulations on the Diffusion of Natural Gas in the Soil for Medium-Pressure Gas Pipeline Leak. *J. Saf. Sci. Technol.* **2014**, *10*, 5–10.
2. Deborah, H.A.; Blanchetière, G.; McCollum, D.; et al. Consequences of a 12 mm Diameter High Pressure Gas Release on a Buried Pipeline. Experimental Setup and Results. *J. Loss Prev. Proc. Ind.* **2018**, *54*, 183–189.
3. Zhu, J.L.; Pan, J.; Zhang, Y.X.; et al. Leakage and Diffusion Behavior of a Buried Pipeline of Hydrogen-Blended Natural Gas. *Int. J. Hydrogen Energy* **2023**, *48*, 11592–11610.
4. Yan, Y.T.; Dong, X.Q.; Li, J.M. Experimental Study of Methane Diffusion in Soil for an Underground Gas Pipe Leak. *J. Nat. Gas Sci. Eng.* **2015**, *27*, 82–89.
5. Latifi, M.; Parvaneh, R.; Naeeni, S.T.O. Investigating the Influence of Surrounding Soil Properties on Leakage Discharge from Cracks in Polyethylene Pipes. *Eng. Fail. Anal.* **2022**, *141*, 106676.
6. Hibi, Y.; Kanou, Y.; Ohira, Y. Estimation of Mechanical Dispersion and Dispersivity in a Soil-Gas System by Column Experiments and the Dusty Gas Model. *J. Contam. Hydrol.* **2012**, *131*, 39–53.
7. Zhang, W.K.; Zhao, G.H. Leakage and Diffusion Characteristics of Underground Hydrogen Pipeline. *Petrol.* **2024**, *10*, 319–325.
8. Peng, S.Y.; Zhang, H.W.; Chai, C.; et al. Effects of Soil Properties on the Diffusion of Hydrogen-Blended Natural Gas from an Underground Pipe. *Fluid Dyn. Mater. Process.* **2025**, *21*, 1099–1112.
9. Liu, Y.L.; Zheng, J.Y.; Xu, P.; et al. Numerical Simulation on the Diffusion of Hydrogen Due to High Pressured Storage Tanks Failure. *J. Loss Prev. Proc. Ind.* **2009**, *22*, 265–270.

10. Yuan, Y.P.; Cui, W.Y.; Tong, L. Prediction and Sensitivity Analysis of Hydrogen Leak Diffusion Using CFD and Data-Driven Modeling under Variable Leak and Wind Conditions. *Int. J. Hydrogen Energy* **2026**, *202*, 153056.
11. Wagih, A.; Oz, F.E.; Melentiev, R.; et al. Advancing Safety of Hydrogen Polymeric Tanks: A Review of Permeation Mitigation, Leak Detection, and Smart Monitoring. *Int. J. Hydrogen Energy* **2025**, *176*, 151334.
12. Wang, X.M.; Hou, T.L.; Gao, W.X.; et al. Experimental Study on the Diffusion Process of Natural Gas from Buried Pipelines to Underground Confined Spaces. *Nat. Gas Ind. B* **2024**, *11*, 603–615.
13. Wang, X.M.; Tan, Y.F.; Zhang, T.T.; et al. Numerical Study on the Diffusion Process of Pinhole Leakage of Natural Gas from Underground Pipelines to the Soil. *J. Nat. Gas Sci. Eng.* **2021**, *87*, 103792.
14. Lyu, S.; Yang, X.B.; Ma, X.Y.; et al. CFD Modeling of Leakage and Dispersion Characteristics of Buried Natural Gas Pipelines—Part 1: Numerical Simulation. *Int. Commun. Heat Mass Transfer* **2026**, *172*, 110351.
15. Ebrahimi-Moghadam, A.; Farzaneh-Gord, M.; Deymi-Dashtebayaz, M. Correlations for Estimating Natural Gas Leakage from Above-Ground and Buried Urban Distribution Pipelines. *J. Nat. Gas Sci. Eng.* **2016**, *34*, 185–196.
16. Ebrahimi-Moghadam, A.; Farzaneh-Gord, M.; Arabkoohsar, A.; et al. CFD Analysis of Natural Gas Emission from Damaged Pipelines: Correlation Development for Leakage Estimation. *J. Clean. Prod.* **2018**, *199*, 257–271.
17. Liu, C.W.; Liao, Y.H.; Liang, J.; et al. Quantifying Methane Release and Dispersion Estimations for Buried Natural Gas Pipeline Leakages. *Process Saf. Environ. Prot.* **2021**, *146*, 552–563.
18. Wang, D.; Liu, P.; Hua, C.G.; et al. Research on Natural Gas Leakage Diffusion of Urban Underground Pipeline and Its Explosion Hazard. *KSCE J. Civ. Eng.* **2023**, *27*, 590–603.
19. Yang, Z.; Li, X.H.; Lai, J.B. Analysis on the Diffusion Hazards of Dynamic Leakage of Gas Pipeline. *Reliab. Eng. Syst. Saf.* **2007**, *92*, 47–53.
20. Hu, Q.F.; Zhang, Z.Y.; Su, Z.; et al. Investigation and Numerical Simulation of a Severe Leakage in an Ultra-Deep Buried Gas Pipeline: A Case Study. *Constr. Build. Mater.* **2025**, *491*, 142745.
21. Zhang, G.W.; An, Z.Y.; Liu, X.P.; et al. Consequence Analysis of Accidental Gas Leak from Storage Tank Group Using LES Method. *J. Loss Prev. Proc. Ind.* **2025**, *94*, 105529.
22. Ikwan, F.; Sanders, D.; Hassan, M. Safety Evaluation of Leak in a Storage Tank Using Fault Tree Analysis and Risk Matrix Analysis. *J. Loss Prev. Proc. Ind.* **2021**, *73*, 104597.
23. Yu, J.X.; Ding, H.Y.; Yu, Y.; et al. Risk Assessment of Liquefied Natural Gas Storage Tank Leakage Using Failure Mode and Effects Analysis with Fermatean Fuzzy Sets and CoCoSo Method. *Appl. Soft Comput.* **2024**, *154*, 111334.
24. Wu, Y.J.; Yang, G.; Sun, J.G.; et al. Digital Twin Modeling and Leak Diagnosis of Temperature and Stress Fields in LNG Storage Tanks. *Measurement* **2024**, *228*, 114374.
25. Xie, Y.S.; Wang, T.; Lv, L.H.; et al. Full-Scale Experiment of Diffusion Behaviors of City Pipeline Gas in Soils. *Nat. Gas Ind.* **2015**, *35*, 106–113.
26. Chen, L.D.; Roquemore, W.W.M.; Goss, L.P.; et al. Vorticity Generation in Jet Diffusion Flames. *Combust. Sci. Technol.* **1991**, *77*, 41–57.
27. Hu, L.; Lu, K.; Delichatsios, M.; et al. An Experimental Investigation and Statistical Characterization of Intermittent Flame Ejecting Behavior of Enclosure Fires with an Opening. *Combust. Flame* **2012**, *159*, 1178–1184.
28. Fang, J.; Wang, J.W.; Guan, J.F.; et al. Momentum- and Buoyancy-Driven Laminar Methane Diffusion Flame Shapes and Radiation Characteristics at Sub-Atmospheric Pressures. *Fuel* **2016**, *163*, 295–303.
29. Goss, L.P.; Katta, V.R.; Roquemore, W.M. Simulation of Vortical Structures in a Jet Diffusion Flame. *Int. J. Numer. Methods Heat Fluid Flow* **1994**, *4*, 413–424.
30. Cetegen, B.M.; Kasper, K.D. Experiments on the Oscillatory Behavior of Buoyant Plumes of Helium and Helium-Air Mixtures. *Phys. Fluids* **1996**, *8*, 2974–2984.
31. Yan, M.Q.; Xu, P.; Li, J.; et al. A Buried Gas Pipeline Leakage Model. *J. Pipeline Syst. Eng. Pract.* **2024**, *15*, 04024046.
32. Zhang, R.H.; Chen, G.H.; Huang, S. A Multiphase Mixture Flow Model and Numerical Simulation for the Release of LPG Underground Storage Tank in Porous Environment. In Proceedings of the ASME 2007 Pressure Vessels and Piping Conference, San Antonio, TX, USA, 22–26 July 2007; Volume 42827, pp. 543–550.
33. Liu, S.X.; Hu, L.H. An Experimental Study on Flame Envelope Morphologic Characteristics of Downward-Orientated Buoyant Turbulent Jet Fires. *Proc. Combust. Inst.* **2019**, *37*, 3935–3942.
34. Zhou, G.; Kong, Y.; Bing, Y.X.; et al. Characterization of Explosion Venting Flame-Shock Wave Coupling Dynamics of LPG/DME Blended Gas under the Influence of Highly Reactive DME. *Combust. Flame* **2025**, *274*, 113980.
35. Coriton, B.; Frank, J.H.; Gomez, A. Effects of Strain Rate, Turbulence, Reactant Stoichiometry and Heat Losses on the Interaction of Turbulent Premixed Flames with Stoichiometric Counterflowing Combustion Products. *Combust. Flame* **2013**, *160*, 2442–2456.
36. Kang, Y.; Cheng, Z.Y. Study on Explosion Characteristics and Consequences of Buried Gas Pipelines. *Process Saf. Prog.* **2025**, *44*, 499–513.

37. Wang, K.; Tao, C.F.; Liu, Q.; et al. An Experimental Investigation of Flame Height and Air Entrainment Rate of Double Jet Fires. *Exp. Heat Transfer* **2018**, *31*, 22–31.
38. Bonnaud, C.; Cluzel, V.; Corcoles, P.; et al. Experimental Study and Modelling of the Consequences of Small Leaks on Buried Transmission Gas Pipeline. *J. Loss Prev. Proc. Ind.* **2018**, *55*, 303–312.
39. Wan, H.X.; Ji, J.; Li, K.Y.; et al. Effect of Air Entrainment on the Height of Buoyant Turbulent Diffusion Flames for Two Fires in Open Space. *Proc. Combust. Inst.* **2017**, *36*, 3003–3010.
40. Dahlgren, R.M.T.; Clifford, H.T. *The Monocotyledons: A Comparative Study*; Academic Press: London, UK/New York, NY, USA, 1982.